Materials Chemistry and Physics 125 (2011) 860–865

Contents lists available at ScienceDirect

Materials Chemistry and Physics

journal homepage: www.elsevier.com/locate/matchemphys

Sulfurization of electrodeposited $CuInSe_2$-based solar cells

M. Valdés [a], A. Goossens [b], M. Vázquez [a,*]

[a] División Corrosión, INTEMA, Facultad de Ingeniería, Universidad Nacional de Mar del Plata, Juan B. Justo 4302 – B7608FDQ Mar del Plata, Argentina
[b] Optoelectronic Materials, Faculty of Applied Sciences, Delft University of Technology, Julianalaan 136, 2628 BL Delft, The Netherlands

ARTICLE INFO

Article history:
Received 5 February 2010
Received in revised form 3 September 2010
Accepted 20 September 2010

Keywords:
Chalcogenides
Annealing
Semiconductors
Electrical properties

ABSTRACT

$CuInSe_2$ (CISe) thin films have been prepared by single-step electrodeposition on top of TCO/TiO_2 and TCO/TiO_2/In_2S_3 coated electrodes. TiO_2 and In_2S_3 have been deposited by spray–pyrolysis. The electrodeposition step is studied using cyclic voltammetry in an acidic electrolyte. Electrodeposited CISe is then subjected to two different thermal treatments. The first treatment is an annealing step under argon atmosphere, carried out to enhance the crystallinity of the film. The second consists of a sulfurization process, where sulfur is vaporized and mixed with the argon flux, leading to substantial changes in the composition of the chalcogenide. The crystallinity, morphology and stoichiometry of the annealed films are characterized by XRD, micro-Raman spectroscopy and SEM/EDX. Raman spectra and EDX show an almost complete replacement of the Se atoms by S atoms. Etching the films in KCN solution is a key step, enabling a final adjustment in the stoichiometry. The incorporation of In_2S_3 buffer layer in TiO_2/$CuIn(SeS)_2$ solar cells produces a marked improvement in the cell efficiency. Despite this improvement, the values of J_{sc} and the fill factor (FF) are relatively low, showing efficiencies below 1%, most likely associated to the resistances present in the multi-layered cell.

1. Introduction

For the last 15 years chalcopyrite compounds have attracted attention due their excellent properties for optoelectronic applications. Along this line, $CuInSe_2$ (CISe) and $CuInS_2$ (CIS) have been under intense research as absorbing materials for terrestrial solar cells. For this kind of application, low cost and large area processing are crucial. Electrodeposition and chemical spray–pyrolysis have emerged as alternative low-cost methods for thin film solar cell production, reaching remarkable conversion efficiencies [1–4].

CISe films electrodeposited from aqueous solutions at room temperature lack sufficient crystallinity. During the subsequent annealing process, recrystallization leads to a considerable reduction of crystallographic defects. During the annealing stage, an oxygen-free atmosphere is necessary to avoid the formation of oxides within the film [5]. Moreover due to the low vapor pressure of Se, films annealed in vacuum, nitrogen or argon atmospheres usually present high levels of Se vacancies [6]. For this reason, various Se sources such as H_2Se or elemental Se are added into the annealing chamber to replace the lost selenium and to adjust the final stoichiometry of the CISe films. However, the high toxicity of gaseous Se can be a limitation for mass production of CISe-devices. To overcome this drawback, one possibility is to transform the $CuInSe_2$ into $CuInSe_{2-x}(S)_x$ by replacing Se sources with S during the annealing step. Further from avoiding the use of Se, an important advantage of this transformation is the increment in the band gap energy of the film from 1.1 eV to 1.4 eV, which yields a closer match between the band gap and the solar spectrum.

Nakamura and Yamamoto [7] were the first to prepare $CuInS_2$ by one-step electrodeposition with post-deposition annealing in N_2 and H_2S and thiosulfate ($Na_2S_2O_3$) as sulfur source. Later, other authors have worked on the electrodeposition of $CuInS_2$ and most of these works deal with a thermal treatment in H_2S [8–13]. There are few publications where the annealing step is performed avoiding the use of highly toxic H_2S [14–16]. Furthermore, there are some drawbacks with the sulfur source used in the electrolyte. Both NH_2SNH_2 and Na_2SO_3 present not well-understood differences regarding the concentration, acidity of the bath and their influence in the final composition of the film. In comparison, there are much more studies on the electrodeposition of $CuInSe_2$, and for this last system, there is a better understanding of the electrochemical processes involving the formation of chalcopyrite. So we have undertaken the electrodeposition of $CuInSe_2$ film with a post sulfurization treatment with molten S to produce a layer of $CuInSe_{2-x}(S)_x$.

Izquierdo-Roca et al. have thoroughly studied the annealing of electrodeposited CISe under sulfurizing conditions by means of Raman spectroscopy [17,18]. They found that if the annealing time is longer than 20 min the chemical composition of the layer changes, resulting in a higher incorporation of sulfur into the chal-

* Corresponding author. Tel.: +54 223 481 6600; fax: +54 223 481 0046.
E-mail address: mvazquez@fi.mdp.edu.ar (M. Vázquez).

0254-0584/$ – see front matter © 2010 Elsevier B.V. All rights reserved.
doi:10.1016/j.matchemphys.2010.09.032

copyrite lattice. Also in the Cu–Se binary phases there is a selective exchange of Se by S, due to their higher reactivity [19].

Our study focuses on the reactive sulfurization taking place during the annealing of $CuInSe_2$ precursor films, which are obtained by electrodeposition on Mo/glass and TCO/TiO_2/In_2S_3 substrates. Two different substrates are used so as to follow and characterize the transformation from CISe to CIS, avoiding the potential interference from the SnO_2 contained in the TCO glass.

2. Experimental procedure

TCO electrodes are degreased in ethanol and rinsed with distilled water during 15 min prior to use. Next TCO squares (2 cm × 2 cm) are placed in a hot plate at 350 °C and coated with TiO_2 using spray–pyrolysis. The precursor solution consists of a mixture of ethanol, titanium isopropoxide and acetylacetone as stabilizer. More details of the spray process can be found in our previous work [20]. After the spraying process, the samples are kept in the hot plate for 30 min at 450 °C to enhance the crystallinity of the TiO_2 film and are then allowed to cool down on the hot plate.

Subsequently a thin layer of In_2S_3 is deposited by spray–pyrolysis at 300 °C on top of the TiO_2 film. This plays the role of a buffer layer in the solar cell prototype. An aqueous solution containing 0.12 mol L^{-1} of thiourea and 0.018 mol L^{-1} of $InCl_3$ is atomized using N_2 as a carrier gas. After the spraying process, the samples are kept on the hot plate at the spraying temperature for 30 min to enhance the crystallization.

$CuInSe_2$ (CISe) is electrodeposited on top of TCO/TiO_2 and TCO/TiO_2/In_2S_3 substrates. The electrolytic bath consists of an aqueous solution containing 2.5×10^{-3} mol L^{-1} $CuCl_2$, 1×10^{-2} mol L^{-1} $InCl_3$ and 5×10^{-3} mol L^{-1} SeO_2. Also, 0.2 mol L^{-1} KCl is used as a supporting electrolyte and the pH is adjusted between 2 and 2.5 using HCl. Potentials ranging from −0.8 to −1.0 V vs. SCE (saturated calomel electrode) are used to study differences in the stoichiometry of the films. The deposition time is always 1 h and the solution is purged with nitrogen to remove the oxygen of the electrolyte before the electrodeposition. After completing the electrodeposition the samples are rinsed with distilled water and dried in air.

To improve the crystallinity of the CISe films, thermal treatments are carried out in a three-temperature zone thermal reactor. This reactor is vacuum pumped and flushed with argon to remove the oxygen inside the quartz tube.

One group of $CuInSe_2$ samples is annealed in argon atmosphere at 500 °C during 30 min. These samples will be referred as "annealed CISe".

A second group undergoes a sulfurization process. This step changes the composition of the film from $CuInSe_2$ to $CuInSe_{2-x}(S)_x$ (with x close to 2), modifying also the optoelectronic properties of the films. First, the samples are placed in the cold zone (T_{amb}) of the tube. Then the second zone is heated to 500 °C and in the third zone the sulfur powder is allowed to reach 300 °C (melting starts at around 200–250 °C). At this point, the samples are moved to the second zone in order to start the sulfurization process, as the vaporized sulfur gets in contact with the samples assisted by the argon flux. After 30 min the samples are cooled down by placing them back in the "cold zone". The samples receiving this treatment will be labeled as CISeS.

Finally to remove secondary phases formed during the electrodeposition or during the thermal treatments (such as CuSe and/or CuS), CISe and CISeS films are etched in 0.5 mol L^{-1} KCN solution during 1 or 5 min.

The crystalline structure of the films is analyzed by X-ray diffraction using a Philips 3020 goniometer with PW 3710 controller, using Cu α radiation and Ni filter at 40 kV and 30 mA. The samples are scanned between 10° and 70° with a step size of 0.01°.

Raman spectroscopy measurements are performed using an Invia Reflex confocal Raman microprobe. Excitation is provided with the 514 nm emission line of an Ar^+ laser and measurements are performed in backscattering configuration using a 50× objective.

The morphology of the layers is studied by scanning electron microscopy (SEM), using a JEOL JSM-6460LV microscope. The composition is analyzed by X-ray energy dispersive spectroscopy (EDS) investigations. The system used is an EDAX Genesis XM4 – Sys 60, equipped with Multichannel Analyzer EDAX mod EDAM IV, Sapphire Si(Li) detector and Super Ultra Thin Window of Be, and EDAX Genesis version 5.11 software.

To investigate the photoelectric response of the cells, current–voltage curves of a solar cell prototype such as TCO/TiO_2/In_2S_3/CISeS/graphite are performed in the dark and under simulated solar irradiation. The graphite contacts are painted onto the samples with conductive graphite ink. Electrode area (0.031 cm^2) is defined using a mask. In all the electrical measurements, the graphite electrode is the working electrode, while the TCO film serves as the counter/reference electrode. Thus, in forward bias, the graphite film is positive relative to the TCO electrode. The light source is a 150 W Xe lamp coupled with a 380 nm UV-filter. The light intensity is evaluated using a Si-photodiode.

3. Results and discussion

The redox reactions of each of the various components of the electrolytic bath can be analyzed by cyclic voltammetry. The voltammograms are recorded at 0.01 V s^{-1} and the potential is scanned first in the negative direction. 0.2 mol L^{-1} KCl is added as supporting electrolyte in order to avoid the effect of having different ionic strengths. TCO coated with a sprayed film of TiO_2 is used as substrate and working electrode.

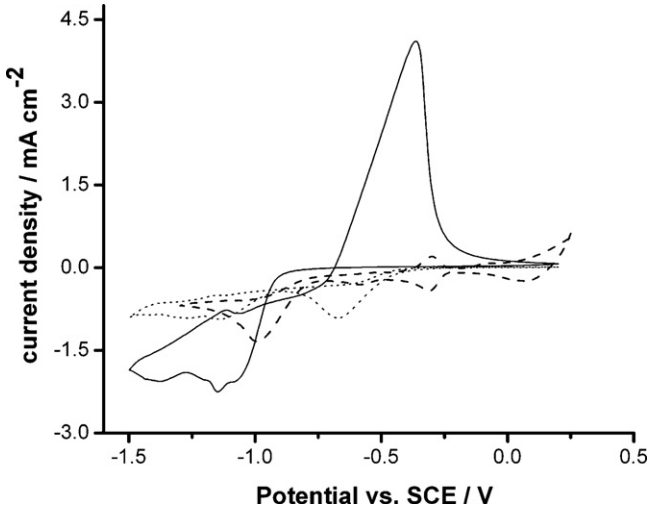

Fig. 1. Cyclic voltammogram of a TCO/TiO_2 coated electrode in 1×10^{-2} mol L^{-1} $InCl_3$ (full line); 2.5×10^{-3} mol L^{-1} $CuCl_2$ (dashed line) and 5×10^{-3} mol L^{-1} SeO_2 (dotted line) precursor electrolytes. Each solution contains 0.2 mol L^{-1} KCl as supporting electrolyte and the pH is adjusted in 2.5 using HCl. The sweep rate is 10 mV s^{-1}.

Fig. 1 shows the voltammograms recorded in three different solutions containing 1×10^{-2} mol L^{-1} $InCl_3$, 2.5×10^{-3} mol L^{-1} $CuCl_2$ and 5×10^{-3} mol L^{-1} SeO_2. Oxidation and reduction currents are higher than those for Cu^{2+} and $HSeO_3^-$ because the concentration of indium ions is higher. In the case of In^{3+}, one reduction and one oxidation peak can be observed (reaction (1)), as has been described before by other authors using SCN^- as complexing agent [9]. Chlorides and thiocianates are well-known complexing agents for indium ions. The potential of the peaks is very similar in both electrolytes, confirming that conductive glass coated with TiO_2 is a suitable substrate.

$$In^{3+}(aq) + 3e^- \leftrightarrows In(s) \quad (1)$$

The voltammogram obtained using the Cu^{2+} solution shows two reduction peaks, one probably corresponding to the formation of Cu^+ (reaction (2a)) and the other to metallic copper formation (reaction (2b)).

$$Cu^{2+}(aq) + e^- \leftrightarrows Cu^+(aq) \quad (2a)$$

$$Cu^+(aq) + e^- \leftrightarrows Cu(s) \quad (2b)$$

In the case of $HSeO_3^-$, also two cathodic peaks appear: the first probably corresponds to the reduction to elemental Se (reaction (3a)) and the second to further reduction to H_2Se (reaction (3b)). The direct comparison of the three voltammograms shown in Fig. 1 presents the following reduction order: $HSeO_3^-$ reduces first, then Cu^{2+} and finally In^{3+}. All three reductions take place between −0.6 and −1.2 V.

$$HSeO_3^-(aq) + 5H^+(aq) + 4e^- \leftrightarrows Se(s) + 3'H_2O \quad (3a)$$

$$Se(s) + 2H + (aq) + 2e^- \leftrightarrows H_2Se(aq) \quad (3b)$$

Fig. 2 illustrates the first, third and fifth cycles of a cyclic voltammogram carried out using a solution containing a combination of all three ions together: 1×10^{-2} mol L^{-1} $InCl_3$, 2.5×10^{-3} mol L^{-1} $CuCl_2$ and 5×10^{-3} mol L^{-1} SeO_2. The first negative scan is very similar than that for $HSeO_3^-$. Apparently Se forms first, then inducing

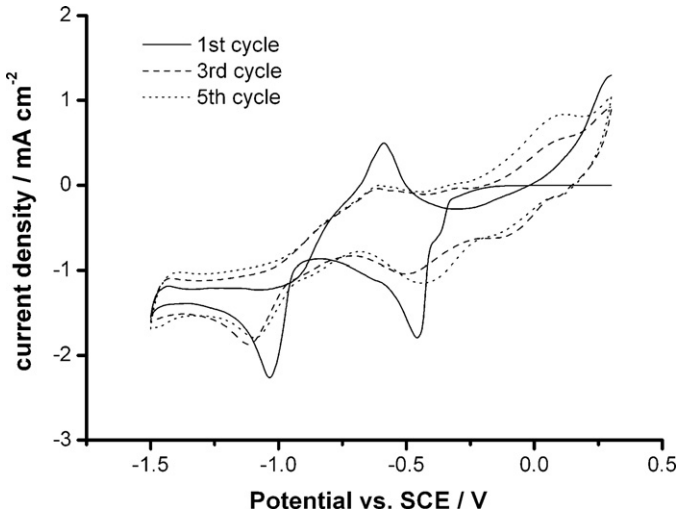

Fig. 2. Cyclic voltammogram of a TCO/TiO_2 coated electrode in the precursor electrolyte containing 2.5×10^{-3} mol L^{-1} $CuCl_2$, 10×10^{-3} mol L^{-1} $InCl_3$, 5×10^{-3} mol L^{-1} SeO_2 and 0.2 mol L^{-1} KCl as supporting electrolyte (pH = 2.5). The sweep rate is 10 mV s^{-1}.

$Cu_{2-x}Se$ formation and finally incorporating In^{3+} into $CuInSe_2$, as suggested before [20]. As more cycles are recorded, the maximum negative current is registered between −0.8 and −1.2 V and so this is the potential range chosen to perform the electrodeposition of CISe. The presence of a thin layer of In_2S_3 placed on top of TiO_2 to complete the solar cell configuration does not present substantial differences in the voltammogram.

Fig. 3 shows typical XRD patterns of electrodeposited CISe films, illustrating the effect of annealing in Ar and S atmosphere. The films were deposited at −1.0 V and using TCO/TiO_2/In_2S_3 substrates. Fig. 3A presents the diffractogram of an as-deposited film, together with CISe (annealed in Ar flush, 30 min at 500 °C) and CISeS (sulfur powder incorporated to the annealing chamber). Without annealing, the main peaks belong to the substrate (SnO_2:F) and anatase from the sprayed TiO_2 films. Annealing significantly improves the crystallinity of the CISe films and the characteristic peaks of the chalcogenide structure, as (1 1 2), (2 0 4) and (2 0 0/1 1 6) can be clearly distinguished in the diffractograms. Also, some other peaks appear that can be attributed to the formation of secondary phases such as CuSe, In_2Se_3 while others are attributed to elemental Se present in the film. Other authors have reported the presence of these secondary phases, detected by XRD analysis [6,17,22]. Finally, after sulfurization, $CuInS_2$ characteristic peaks appear in the diffractogram, while the peaks corresponding to $CuInSe_2$ can no longer be seen. This can be interpreted by the replacement of Se atoms by S atoms during the sulfurization step. Furthermore the sulfurization seems to reduce the amount of secondary phases in the film in comparison to the annealing in argon.

The presence of remnant CISe after sulfurization is difficult to identify because the main reflection of the (1 1 2) of the $CuInSe_2$ at 26.6° (JCPD N° 40-1487) is too close to that of the SnO_2 main peak at 26.48° (JCPD N° 77-0452). Mo glass has been used as substrate in order to avoid the interference of SnO_2 (from TCO glass). When using Mo coated glass, the main peaks of CISe and CIS are well separated from those of the substrate, so Fig. 3B can be taken as evidence that the sulfurization step changes the composition of the electrodeposited layer, replacing Se atoms by S atoms. No peaks that could be attributed to $CuInSe_2$ are present after sulfurizing film. Fig. 3C shows a magnification of the change in the (1 1 2) diffraction plane from the CISe structure to the CIS structure, after sulfurization.

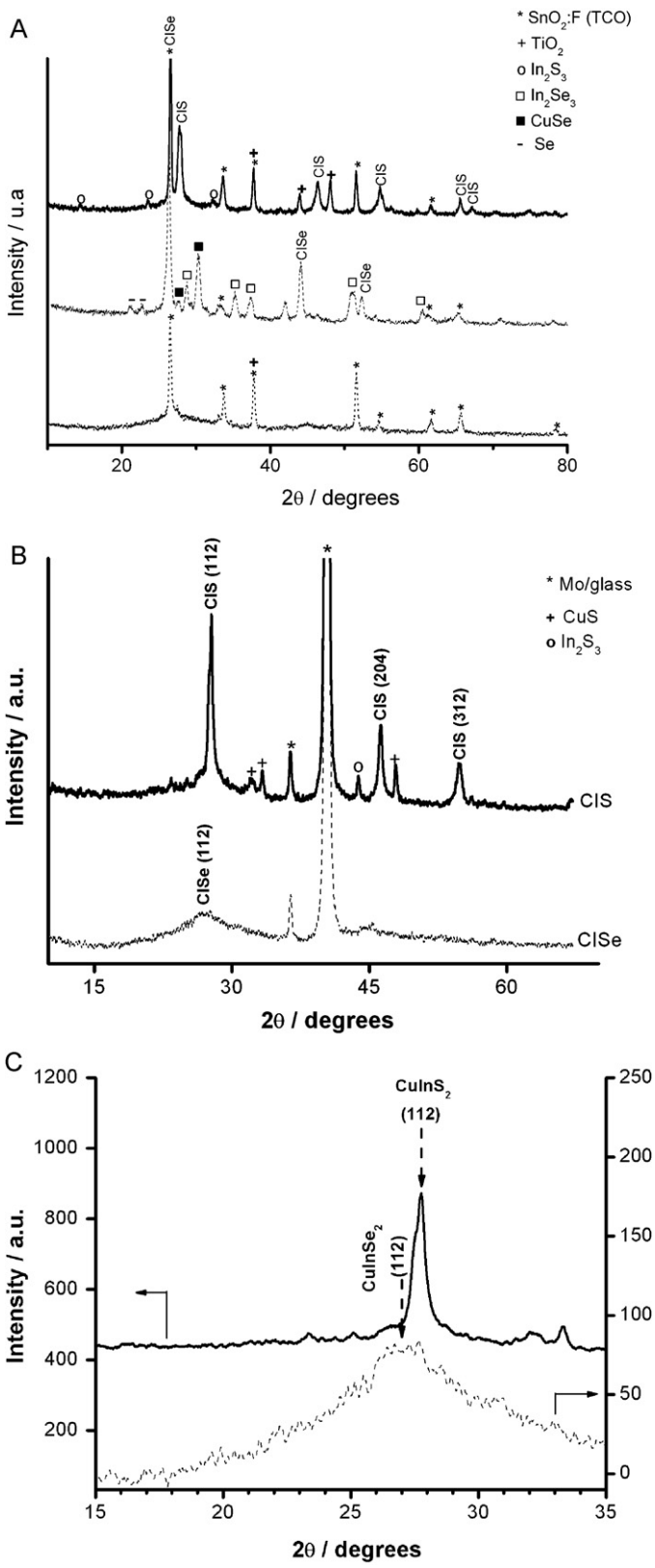

Fig. 3. X-ray diffractogram of CuInSe electrodeposited on (A) TCO/TiO_2/In_2S_3 electrode. From bottom to top the diffractograms represent an as-deposited sample, a sample annealed in Ar (CISe) and a sample annealed in S (CISeS) and (B) X-ray diffractogram of CuInSe electrodeposited on Mo/glass electrode showing the change of the crystalline structure before (bottom) and after (top) the sulfurization process. (C) magnification of the (1 1 2) diffraction plane.

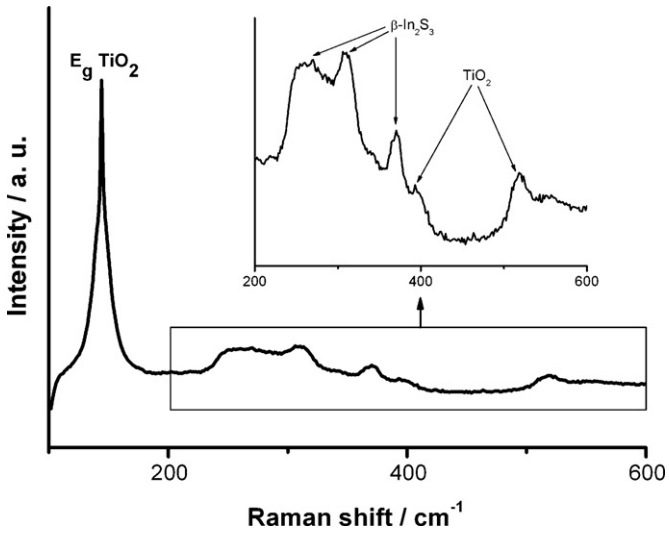

Fig. 4. Raman spectrum of the TCO/TiO_2/In_2S_3 substrate. The TiO_2 and In_2S_3 thin films are deposited by chemical spray–pyrolysis. The inset in the graph shows a magnification displaying characteristic indium sulfide modes.

A Raman spectrum of the TCO coated with TiO_2 and In_2S_3 is presented in Fig. 4. The spectrum contains a well-defined signal at 144 cm^{-1} corresponding to the main vibration mode of anatase (TiO_2). Other anatase modes and indium sulfide modes appear between 200 and 600 cm^{-1} and are identified in the inset of the graph.

A Raman spectrum of as-deposited CISe is shown in Fig. 5 presenting the main vibration modes of the $CuInSe_2$ structure [23]. The asterisk denotes a signal coming from the TiO_2 layer below and the arrow indicates a low frequency shoulder in the 154 cm^{-1} region related to complex point defects in the chalcopyrite structure leading to the formation of ordered vacancies compounds (OVCs), as is reported in the literature [17,24].

The effect of the sulfurizing process, together with the effect of annealing, has also been investigated by Raman spectroscopy, shown in Fig. 6. Although the intensity of the Raman signal depends on the surface morphology and the phases present within the CISe films, all the spectra contain the A_1 mode between 172 and 178 cm^{-1} related to the vibration of Se–Se bonds (anions) and a peak at 120 cm^{-1} of the Cu–In bonds (cations). In the case of annealed CISe an additional peak at 263 cm^{-1} can be seen. The latter peak is related to the presence of a Cu_xSe secondary phase. After sulfurizing, the A_1 mode shifts to the A_1 frequency of the $CuInS_2$ at 292 cm^{-1}, confirming the partial transformation of CISe into CISeS. Moreover, a new peak appears at 470 cm^{-1}. This can be related to Cu_xS compounds and can be taken as a proof that the Cu_xSe secondary phase is transformed during the annealing in sulfur, changing its composition. A well-known method to remove the Cu_xSe and Cu_xS phases is etching the film in KCN solutions. After using KCN 0.5 mol L^{-1} for 5 min, the spectrum (Fig. 6) shows the dissolution of the secondary phases, with only CISe and CIS vibration modes still present.

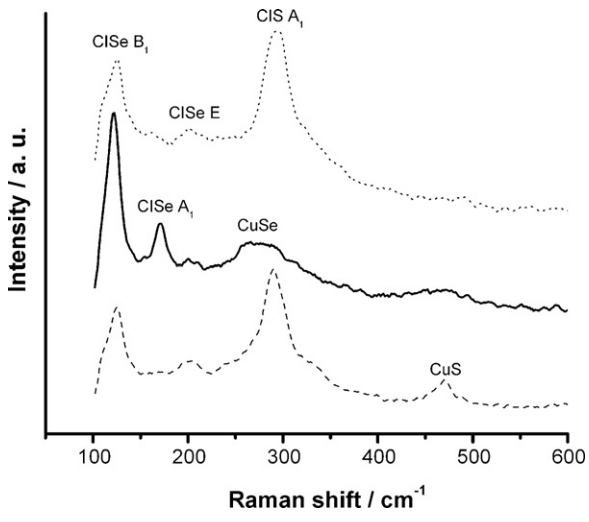

Fig. 6. Raman spectra of CISe and CISeS films. (Full line) CISe film annealed in argon at 500 °C during 30 min (dashed line) CISeS sulfurized at 500 °C during 30 min and (dotted line) CISeS sulfurized at 500 °C during 30 min and etched in 0.5 mol L^{-1} KCN for 5 min.

A more detailed Raman spectrum of CISeS is shown in Fig. 7. The deconvolution of the spectrum allows the identification of characteristic modes of the $CuInS_2$ structure, such as the previously mentioned A_1 mode (292 cm^{-1}) and a signal at 470 cm^{-1} related to the presence of covallite (CuS) structure. Additional modes are found: a low frequency signal at 240 cm^{-1} can be assigned to the E vibration mode, a signal at 305 cm^{-1} can be caused by the presence of Cu–Au ordering [25,26] and a signal at 337 cm^{-1} assigned to the contribution from the modes of the $CuIn_5S_8$ spinel-type structure.

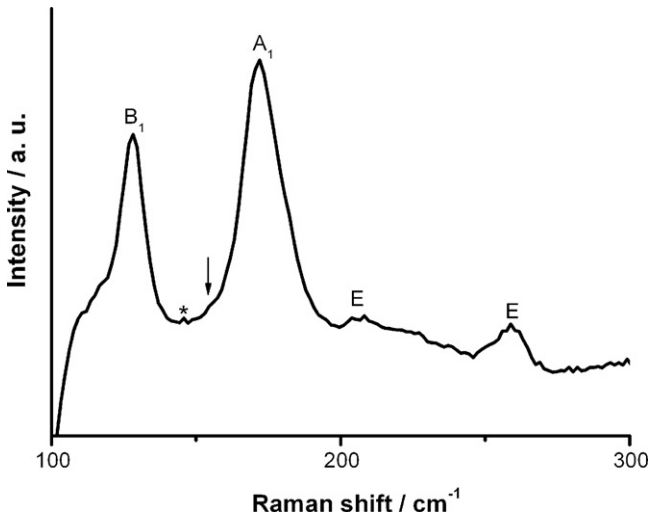

Fig. 5. Raman spectrum of as-deposited CISe at −0.8 V vs. SCE during 1 h.

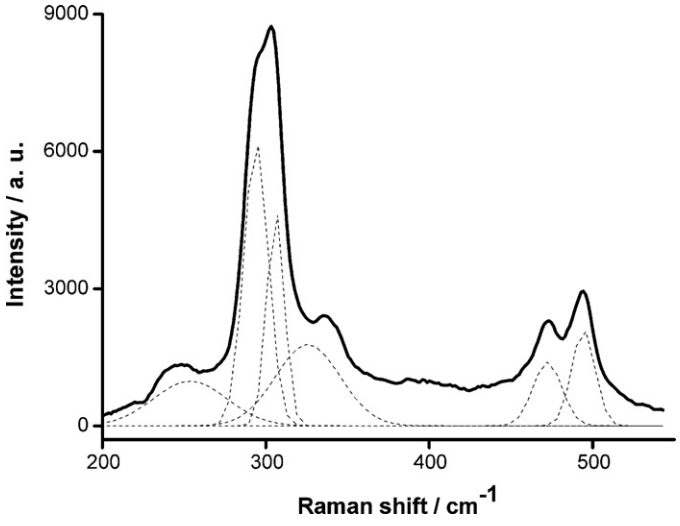

Fig. 7. Raman spectrum of CISeS deposited at −1 V and sulfurized at 500 °C during 30 min. The doted lines represent the deconvolution of the spectrum.

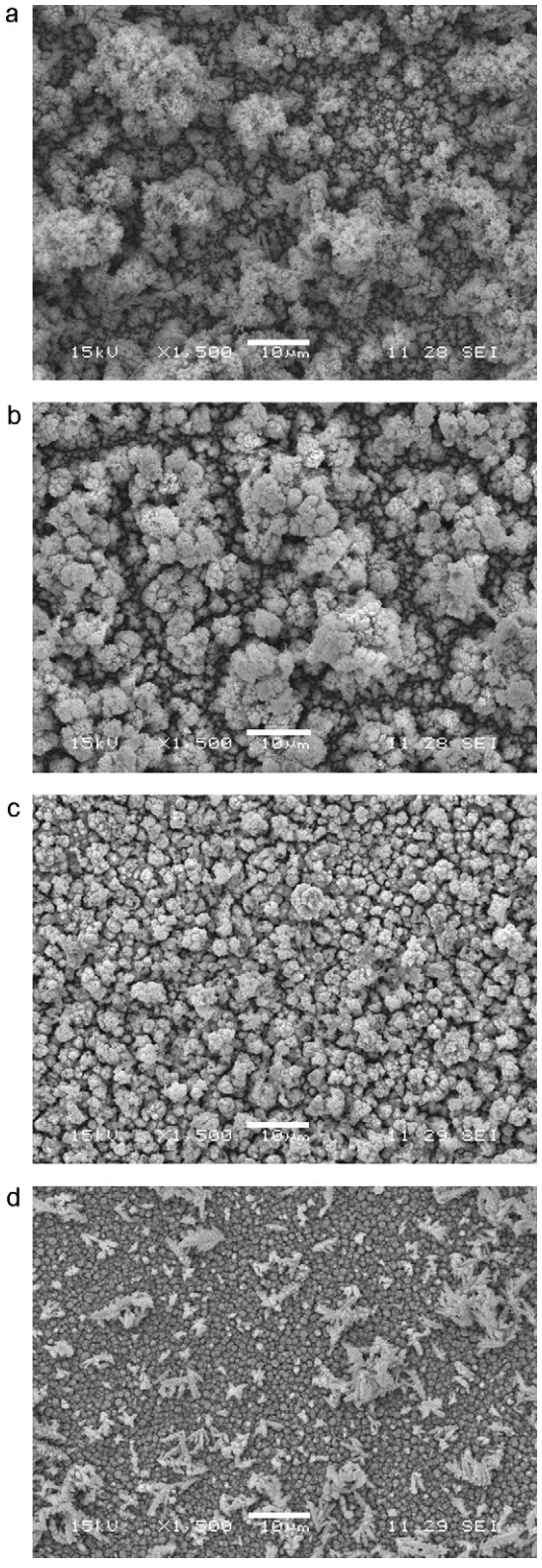

Fig. 8. SEM images of $CuInSe_2$ films deposited on TCO/TiO_2 electrodes at −1 V vs. SCE during 1 h: (a) as-deposited, (b) annealed in argon 30 min at 500 °C in argon atmosphere, (c) sulfurized 30 min at 500 °C and etched in KCN solution during 1 min and (d) sulfurized 30 min at 500 °C and etched in KCN solution during 5 min.

This type of structure is more likely to be present in In-rich composition [19]. Also, according to Izquierdo-Roca et al. [17] the high frequency signal at 495 cm^{-1} could be attributed to the S–S vibration mode, indicating the replacement of Se atoms by S atoms in the lattice of the chalcopyrite phase.

Table 1
Elemental composition of CISe films deposited on TCO/TiO_2 electrodes at −1 V vs. SCE during 1 h with different treatments.

Deposition	Thermal treatment	KCN etching	EDX (%)			
			Cu	In	Se	S
−1 V vs. SCE/1 h	x	x	32.3	22.0	45.6	
−1 V vs. SCE/1 h	Annealed	x	36.8	20.6	42.6	
−1 V vs. SCE/1 h	Sulfurized	1 min	26.1	22.8	8.4	42.6
−1 V vs. SCE/1 h	Sulfurized	5 min	18.5	26.8	8.4	46.2

The processes of sulfurizing and etching the samples have also been followed by scanning electron microscopy. SEM photographs taken on as-deposited samples, together with CISe, CISeS and etched CISeS are presented in Fig. 8. As can be seen in the sequence from Fig. 8a–d, after 5 min of etching the relative amount of secondary phases is greatly reduced. The elemental composition obtained by EDX is presented in Table 1. As can be seen the annealing in argon reduces the indium and selenium content in the samples due to the low vapor pressure of these elements. The cross-section image (Fig. 9) is included to illustrate average thicknesses of the TiO_2 film (0.3 μm), buffer layer (0.5 μm) and the CISeS absorbing layer (2.6 μm).

Fig. 10 presents the *I–V* response of a TCO/TiO_2/CISeS/graphite configuration (cell 1). The CISeS is electrodeposited at −1.0 V for 1 h,

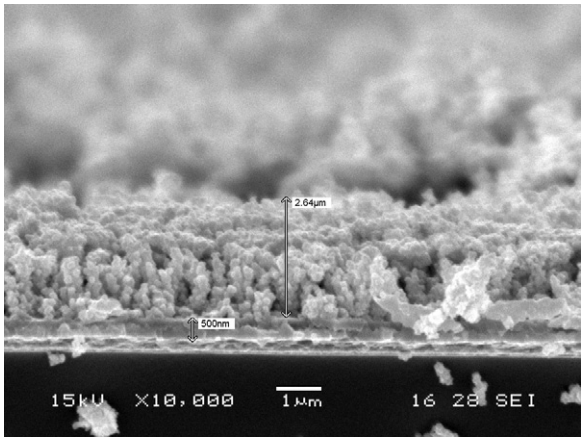

Fig. 9. Cross sectional view of a $CuInSe_2$ electrodeposited on TCO/TiO_2/In_2S_3 electrode at −1 V vs. SCE during 1 h.

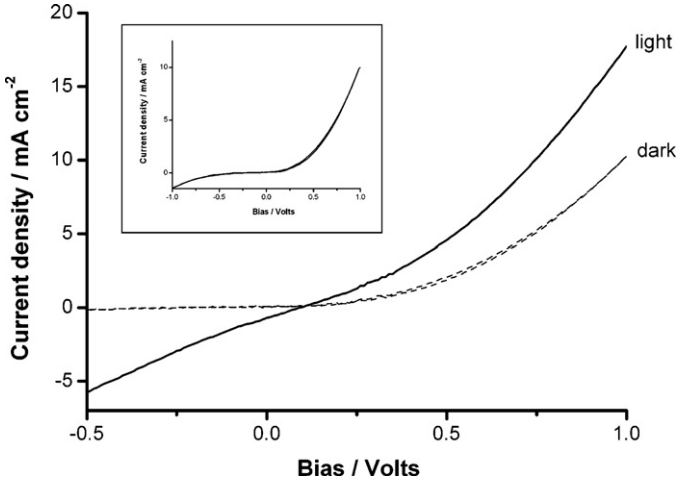

Fig. 10. *I–V* response of a TCO/TiO_2/CISeS/graphite cell configuration (cell 1) in the dark and under simulated solar irradiation. The CISeS film is sulfurized and etched 5 min in KCN solution. The inset shows the complete diode response of the device.

Table 2
Characteristic parameters of the solar cells under study.

	I_{sc} (mA cm^{-2})	V_{oc} (V)	FF	η (%)
Cell 1	−0.69	0.095	0.26	0.024
Cell 2	−2.31	0.365	0.25	0.3

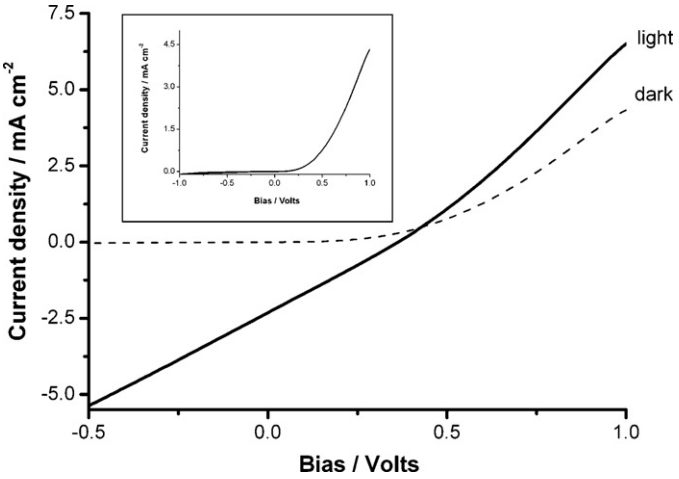

Fig. 11. *I–V* response of a TCO/TiO_2/In_2S_3/CISeS/graphite cell configuration (cell 2). The CISeS film is sulfurized and etched 5 min in KCN solution. The inset shows the complete diode response of the device.

sulfurized and finally etched in KCN solution (5 min). The characteristic parameters of the cell are shown in Table 2. The low value of the I_{sc}, V_{oc} and FF can be attributed to a fast hole–electron recombination in the interface as was reported in our previous works [20,21]. In most chalcopyrite solar cells, a buffer layer is typically required between the n-type and p-type regions to control the interfacial properties [4,27,28]. Adding a thin In_2S_3 layer significantly improves (in a factor of 10) the efficiency, as can be seen in Fig. 11 and Table 2 (cell 2) for a TCO/TiO_2/In_2S_3/CISeS/graphite cell configuration.

Despite the improvement, the values of I_{sc} and fill factor are still very low and do not reach efficiencies comparable with other chalcopyrite-based multilayer devices [3,4,18]. The low FF and I_{sc} values are frequently associated with the presence of pinholes and also to series and shunt resistances present in the multilayer structure. The incidence of pinholes could be reduced by depositing thicker films but this, in turn, would be detrimental to the overall resistance of the layered structure. Current investigations aim at determining the films resistance and at finding optimal thickness values, so as to improve the cell performance.

Also, as argued by Saucedo et al. [19], CuS binary aggregates formed deep into the CISeS layer may not be reached during the etching stage. Moreover, a spinel-type phase might be formed, which these authors associate to an S–S mode peak at 340 cm^{-1}. This is an n-type phase and could originate a back diode and be partially responsible for the low efficiency of the solar cells.

4. Conclusions

Thin films of $CuInSe_2$ are prepared by single-step electrodeposition on TCO substrates coated with TiO_2 and TiO_2/In_2S_3 layers.

As-deposited and thermally treated films are studied and characterized using XRD, micro-Raman spectroscopy and SEM/EDS analysis. The difference between two different thermal treatments, "annealing in argon" and "sulfurization" has been established and the replacement of Se by S in the structure is evident. Combining the sulfurization process with etching the films in KCN solution, seems to be beneficial, enabling a final adjustment in the stoichiometry of the films and also enhancing the crystallinity of the material. The etching time is an important parameter that influences the final Cu/In ratio in the film.

Finally the incorporation of an In_2S_3 buffer layer in TiO_2/CISeS solar cells devices, produces an improvement in a factor of 10 in the cell efficiency. Despite this improvement, the values of J_{sc} and V_{oc} as well as the fill factor (FF) are relatively low, showing efficiency lower than 1%. Further investigations will be focused on improving the cell efficiency by lowering the resistances associated to the multi-layered cell. In parallel, electrochemical etching is currently being explored, in order to attack detrimental secondary phases formed deep into the absorber layer that cannot be reached by the KCN etching solution.

Acknowledgements

The authors acknowledge the financial support received from Consejo Nacional de Investigaciones Científicas y Técnicas (CONICET), Agencia Nacional de Promoción Científica y Tecnológica (ANCyPT), Universidad Nacional de Mar del Plata (UNMdP) and the Technological University of Delft (TUDelft).

References

[1] P.J. Sebastian, M.E. Calixto, R.N. Bhattacharya, R. Noufi, J. Electrochem. Soc. 145 (1998) 3613.
[2] D. Lincot, J.F. Guillemoles, S. Taunier, D. Guimard, J. Sicx-Kurdi, A. Chaumont, O. Roussel, O. Ramdani, C. Hubert, J.P. Fauvarque, N. Bodereau, L. Parissi, P. Panheleux, P. Fanouillere, N. Naghavi, P.P. Grand, M. Benfarah, P. Mogensen, O. Kerrec, Sol. Energy 77 (2004) 725.
[3] T.T. John, M. Mathew, C.S. Kartha, K.P. Vijayakumar, T. Abe, Y. Kashiwaba, Sol. Energy Mater. Sol. Cells 89 (2005) 27.
[4] M. Nanu, J. Schoonman, A. Goossens, Nano Lett. 5 (2005) 1716.
[5] K.T.L. De Silva, W.A.A. Priyantha, J.K.D.S. Jayanetti, B.D. Chithrani, W. Siripala, K. Blake, I.M. Dharmadasa, Thin Solid Films 382 (2001) 158.
[6] O. Volobujeva, J. Kois, R. Traksmaa, K. Muska, S. Bereznev, M. Grossberg, E. Mellikov, Thin Solid Films 516 (2008) 7105.
[7] S. Nakamura, A. Yamamoto, Sol. Energy Mater. Sol. Cells 49 (1997) 415.
[8] R.N. Bhattacharya, D. Cahen, G. Hodes, Sol. Energy Mater. 10 (1984) 41.
[9] G. Hodes, T. Engelhard, D. Cahen, L.L. Kazmerski, C.R. Herrington, Thin Solid Films 128 (1985) 93.
[10] C.D. Lokhande, G. Hodes, Sol. Cells 21 (1987) 215.
[11] K.R. Murali, T.N. Suresh Kumar, V. Subramanian, K. Gurunathan, N. Rangarajan, A.S. Lakshmanan, Bull. Electrochem. 12 (1996) 162.
[12] S. Nakamura, Proceedings of the 3rd World Conference on Photovoltaic Energy Conversion, 2003, p. 422.
[13] R.P. Wijesundera, W. Siripala, Sol. Energy Mater. Sol. Cells 81 (2004) 147.
[14] B. Asenjo, A.M. Chaparro, M.T. Gutiérrez, J. Herrero, Thin Solid Films 511–512 (2006) 117.
[15] A.M. Martinez, A.M. Fernández, L.G. Arriaga, U. Cano, Mater. Chem. Phys. 95 (2006) 270.
[16] R. Cayzac, F. Boulch, M. Bendahan, P. Lauque, P. Knauth, Sci. Mater. Eng. B 157 (2009) 66.
[17] V. Izquierdo-Roca, A. Pérez-Rodríguez, A. Romano-Rodríguez, J.R. Morante, J. Ãlvarez-García, L. Calvo-Barrio, V. Bermudez, P.P. Grand, O. Ramdani, L. Parissi, O. Kerrec, J. Appl. Phys. 101 (2007).
[18] V. Izquierdo-Roca, X. Fontané, L. Calvo-Barrio, A. Pérez-Rodríguez, J.R. Morante, J. Álvarez-García, F. Duault, L. Parissi, V. Bermúdez, Thin Solid Films 517 (2009) 2264.
[19] E. Saucedo, V. Izquierdo-Roca, C.M. Ruiz, L. Parissi, C. Broussillou, P.P. Grand, J.S. Jaime-Ferrer, A. Pérez-Rodríguez, J.R. Morante, V. Bermúdez, Thin Solid Films 517 (2009) 2268.
[20] M. Valdés, M. Vázquez, A. Goossens, Electrochimica Acta 54 (2008) 524.
[21] M. Valdés, M.A. Frontini, M. Váquez, A. Goossens, Appl. Surf. Sci. 254 (2007) 303.
[22] C. Guillén, M.A. Martínez, J. Herrero, Vacuum 58 (2000) 594.
[23] C. Rincón, F.J. Ramírez, J Appl. Phys. 72 (1992) 4321.
[24] C. Rincón, S.M. Wasim, G. Marín, J.M. Delgado, J.R. Huntzinger, A. Zwick, J. Galibert, Appl. Phys. Lett. 73 (1998) 441.
[25] J. Álvarez-García, A. Pérez-Rodríguez, B. Barcones, A. Romano-Rodriguez, J.R. Morante, A. Janotti, S.H. Wei, R. Scheer, Appl. Phys. Lett. 80 (2002) 562.
[26] M. Nanu, J. Schoonman, A. Goossens, Thin Solid Films 451–452 (2004) 193.
[27] R. O'Hayre, M. Nanu, J. Schoonman, A. Goossens, Nanotechnology 18 (2007).
[28] M. Krunks, A. Katerski, T. Dedova, I. Oja Acik, A. Mere, Sol. Energy Mater. Sol. Cells 92 (2008) 1016.